A Density Functional Theory Study for the Adsorption of Various Gases on a Caesium-Exchanged Trapdoor Chabazite

Jin Shang[a,b]*, Gang Li[c], Paul A. Webley[a,b]*, and Jefferson Z. Liu[d]*

[a]Cooperative Research Centre for Greenhouse Gas Technologies

[b]Department of Chemical and Biomolecular Engineering, The University of Melbourne, Victoria 3010, Australia

[c]School of Mechanical and Chemical Engineering, The University of Western Australia, Crawley, WA 6009, Australia

[d]Department of Mechanical and Aerospace Engineering, Monash University, Clayton, Victoria 3800, Australia

Corresponding authors: jin.shang@unimelb.edu.au, Tel: +61 3 83446640; paul.webley@unimelb.edu.au, Tel: +61 3 90357873; zhe.liu@monash.edu, Tel: +61 3 990 53627

Abstract

Rational design and development of porous materials for adsorptive gas separation gains ever-increasing attention as industrial applications, such as carbon capture and natural gas purification, always require more energy-efficient processes with adsorbents providing high selectivity. Zeolite molecular sieves represent a class of such desirable adsorbents. Our recently discovered molecular trapdoor mechanism in zeolites allows for unprecedented high selectivity and affords designability for versatile adsorbents. In this work, we presented a route for identifying the molecular trapdoor mechanism and predicting the gas separation feasibility using density functional theory calculations, based on a typical molecule trapdoor zeolite – caesium-exchanged chabazite with silicon to aluminium ratio of 3. We established criteria to assess the viability for "door-open" process by examining the dependence of energy barriers for the movement of "door-keeping" cation in the presence of different gases. Calculations at the standard PBE level and the van der Waals DFT levels were carried out. This theoretical route could serve as a standard method to study and develop other molecular trapdoor zeolites.

Keywords: chabazite zeolite · adsorption · molecular trapdoor · DFT

1. Introduction

Gas separations using microporous materials represents an ever-booming field, especially in recent years, as carbon capture attracts increasing attention due to the pressing concern on energy crisis and environmental protection [1, 2]. For carbon capture, such an energy-efficient process requires high-performance adsorbents to selectively remove CO_2 from other molecules such as N_2, CH_4, H_2, and O_2. Zeolites serve as a primary class of candidate adsorbents for large-scale gas separations owning to multiple advantages such as high selectivity, low cost, as well as high thermal and mechanical stability [3]. These highly porous aluminosilicates possess three-dimensional structure of molecular dimension, thus being known as "molecular sieves". They could yield extremely high selectivity attributed to the molecular sieving effect: the host admits small guests in but excludes large ones out through its pore aperture [4].

However, this conventional explanation for the molecular sieving mechanism deserves a closer scrutiny when accounting for a host aperture coordinated by extraframework cations. In this case, a molecular trapdoor mechanism provides a more reasonable picture: a cation-kept zeolite aperture only exclusively admits certain molecules regardless of size [5-7]. We demonstrated this mechanism by investigating CO_2, N_2, and CH_4 separation on chabazite zeolites. Chabazite [8, 9] features eight-membered ring (8MR) apertures that act as its only access for guest molecules; but in specifically tailored chabazites the guests are blocked by extraframework cations such as K^+ and Cs^+, which coordinate energetically favourably in the center of the 8MRs. For a guest molecule to enter the supercavity, the door-keeping cation has to move away from the center of the 8MR aperture. Our previous studies showed that CO_2 has "stronger" interaction strength with the door-keeping cations than N_2 and CH_4 molecules and thus can significantly flatten the potential well of the cation. At a certain temperature (corresponding to a certain kinetic energy value for the cation), the thermal excitation would lead to the temporary and reversible deviation of the cations away from the center of the 8MR, giving way to CO_2 molecules to hop into the adjacent cages.

This novel molecular trapdoor mechanism opens up a new avenue for designing microporous materials with steered selectivity. However, a rational design requires detailed understanding at the atomic level, aside from trial and error procedures in the lab. Computer simulations provide indispensable tools to investigate and predict the physical chemistry properties at the

atomic level. In this work, we employed density functional theory (DFT) calculations to study the molecular trapdoor mechanism occurring to a Cs-exchanged chabazite. Three typical small size gas molecules, CO_2, N_2, and CH_4 which are relevant to carbon capture applications, were adopted in our theoretical study. We established criteria to assess the viability of "door-open" process. In the end of this manuscript, the criteria were used to predict the selective adsorption of several other small gas molecules in the trapdoor chabazite. This work could afford a standard route for the theoretical design of the molecular trapdoor materials.

2. Methods

2.1 Structure Model Setup

Chabazite [8] consists of double-six ring (D6R) units arranged in layers that are linked together by tilted 4-membered rings (4MRs). The three-dimensional pore structure comprises large ellipsoidal supercavities of 6.7 × 10 Å, each of which is accessed by six eight-membered rings (8MRs) of 3.8 × 3.8 Å (Fig. 1). Previous studies [10-12] have shown that four types of general extraframework cation sites exist in dehydrated chabazite: one at the centre of the D6R prism (SI), one at the triad axis of the D6R prism but displaced to the supercavity (SII), one in the supercavity at the corner of the 4MR window of the D6R (SIII), and one at the center of the 8MR window (SIII').

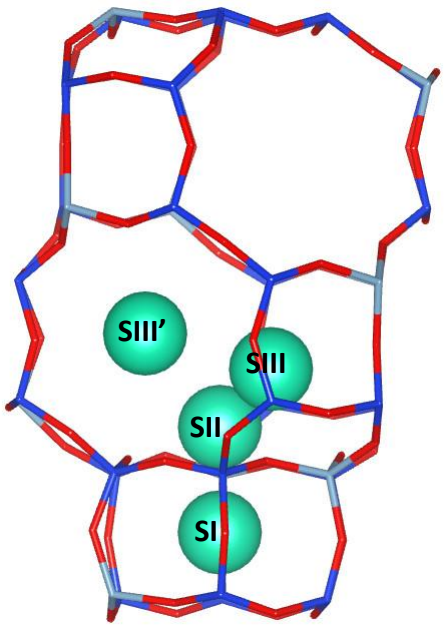

Fig. 1. Schematic representation of chabazite crystal structure and the extraframework cation sites. Double-six ring prisms (D6Rs) connected by tilted four-membered rings (4MRs) form a three-dimensional structure, generating eight-membered rings (8MRs) as the only access to the crystal interior. Four sites exist for extraframework cations: inside the center of a D6R (SI); inside the supercavity above a D6R (SII); inside the supercavity next to a 4MR (SIII); in the center of an 8MR (SIII'). Color scheme: Red, O; Blue: Si; Grey, Al; Aqua, Cs.

Pure-silica chabazite was adopted as the starting point where the structural parameters for a conventional unit cell (referred to as unit cell hereafter), which consists of three double six-ring prisms or one and a half chabazite supercages, were taken from an experimental work [13]. Specifically, a = 13.92779 Å, b = 13.94511 Å, c = 15.12131 Å, α = 90.0929^{o}, β = 89.9757^{o}, γ = 120.3650^{o}. To introduce extraframework cations such as K^+ and Cs^+ into chabazite, a certain amount of silicon atoms were replaced by aluminium atoms to generate negatively charged chabazite frameworks with Si/Al ratio of 35:1 (**r35**CHA) and 3:1 (**r3**CHA), respectively. The unit cell formula is $K_1[Al_1Si_{35}O_{72}]$) for **r35**KCHA, $Cs_1[Al_1Si_{35}O_{72}]$) for **r35**CsCHA, and $Cs_9[Al_9Si_{27}O_{72}]$ for **r3**CsCHA. In our study, the **r35**CHA was used to determine cation site preference, which could be directly compared with literature results. The **r3**CHA represents our experimentally investigated chabazite counterpart, in which the trapdoor mechanism is enabled by considering the cations at relevant sites (SIII') [5].

Given that the Al atoms introduce negative charges into chabazite frameworks, the extraframework cations were initially placed at the cation sites in the vicinity of Al atoms in our DFT calculations. For either **r35**KCHA or **r35**CsCHA, since there is only one Al per unit cell, we placed this Al at an intersection of an 8MR, a 6MR, and a 4MR. This allows us to generate a structure with a K^+ or Cs^+ cation placed at each of the possible cation sites (see Figure 1 for details). By comparing the total energy results (E_{total}) of the obtained different crystal structures, i.e., the total energy with the cation at site SI (E_{total}(SI)), the total energy with the cation at site SII (E_{total}(SII)), E_{total}(SIII), and the total energy with the cation at site SIII' (E_{total}(SIII')), we could determine the site preference as per the rule, i.e., a higher total energy value indicates an unfavourable cation site. In the case of **r3**CsCHA, there are many different ways to place the 9 Al atoms in one unit cell. In order to calculate the energy barrier

for Cs^+ cation migrating from site SIII' to site SII with different number of Al atoms in the corresponding 8MRs and 6MRs, we considered all the possible Al distributions (Figure 5).

For the gas-chabazite complex calculations, the structures were generated by placing a certain loading of gas molecules next to the target cations in supercavities of chabazite crystals. The gas molecule positions were selected so that both cation-gas and gas-gas distances were approximately 3.0 Å.

2.2 Computational Setup

Ab initio density functional theory (DFT) calculations were employed to determine the chabazite structure, cation location and occupancy, as well as gas adsorption configuration. We used the Vienna *Ab initio* Simulation Package (VASP) [15] with the generalized gradient approximation (GGA) [16] and the projector augmented waves (PAW) approach [17]. The cut-off energy of the plane wave basis-set was 600 eV. A gamma point only k-point mesh was used for one unit cell of chabazite (including three double-six ring prisms or one and a half chabazite supercage). Such cut-off energy and k-point mesh have been tested to ensure the total energy convergence within 1 meV/atom. The atomic positions were optimized with the conjugate gradient method until the forces acting on atoms were below 0.015 eV/Å, as suggested by Göltl and Hafner [14]. We applied the nudged-elastic-band (NEB) method [22] for energy barrier calculations.

For the bare chabazite systems, the crystal structure were fully relaxed at PBE level since the dominant interaction in chabazite is the covalent bonding between silicon/aluminium and oxygen atoms and van der Waals dispersion interactions do not play an important role [14]. To more accurately account for the van der Waals interaction in the gas-chabazite complexes, dispersion-corrected DFT calculations with the optB86b-vdW functional scheme [18-20] was adopted because this scheme was determined to be the most appropriate one in our gas-chabazite system in a previous study [21]. Note that in our optB86b-vdW functional calculations, the gas-chabazite complexes fully relaxed at the PBE level were taken as the starting point.

3. Results and Discussion

3.1 Validation of Chabazite Model

We tested our chabazite model system by comparing the K^+ cation site preference in **r35**KCHA with those reported in literatures. This Si/Al ratio corresponds to replacing only one Si atom by one Al atom in one unit cell, which can be taken as a dilute exchanging case. Figure 2 shows the relative total energy of the **r35**KCHA with the K^+ cation located at different sites. Clearly, the K^+ cation favours to reside at these sites in a sequence SIII' > SII > SIII > SI, which agrees with a previous simulation study [23]. We can rationalize the site preference by considering the possible coordination numbers between K^+ cation and framework O atoms. A higher coordination number often leads to a more stable configuration [24]. As shown in Fig. S1: K^+ could coordinate with eight O atoms at site SIII' (Fig. S1a), six at site SII (Fig. S1b), four at site SIII (Fig. S1c), and twelve at site I (Fig. S1d). Note that the highest coordination number at site SI does not lead to the most stable configuration rather the least stable because the volume enclosed in the D6R is too small for the K^+ cation.

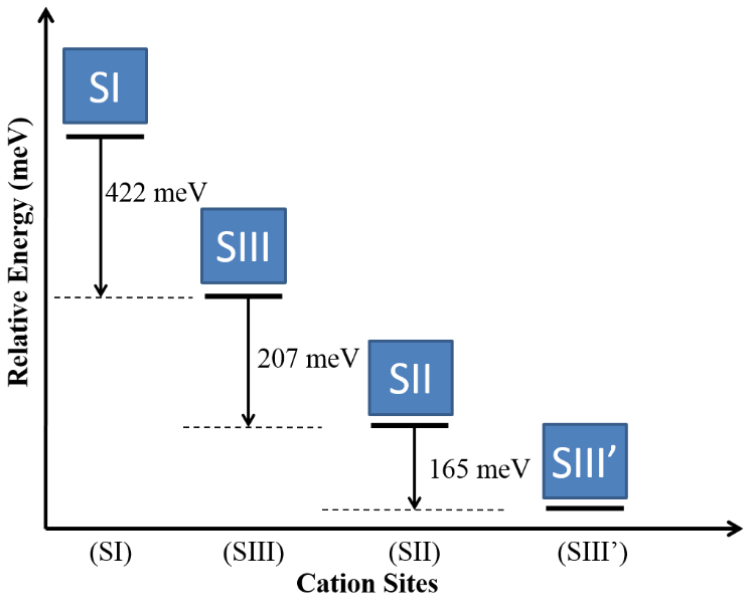

Fig. 2. Relative total energy of **r35**KCHA crystals with K^+ cation located at different sites. Cleary the site SIII' is the most stable cation site for K^+.

3.2 Determination of Cs^+ Cation Site Preference

On the basis of the verified chabazite model – **r35**KCHA, we built **r35**CsCHA by simply replacing K^+ with Cs^+ and investigated the Cs^+ cation site preference. Note that site I was not

considered because of the large size of Cs^+ cation: a diameter of about 3.33 Å in comparison with 6MR window size of about 2.6 Å [5]. Figure 3 shows the relative total energy of **r35**CsCHA with Cs^+ cation at different sites. It shows a site preference in a similar way to K^+ cation, namely, SIII' > SII > SIII. The energy difference between site SIII' and SII is also similar, 159 meV for **r35**CsCHA and 165 meV for **r35**KCHA. But the **r35**CsCHA has a smaller total energy difference for Cs^+ cation occupying SIII and SII than **r35**KCHA, 53 meV vs. 207 meV.

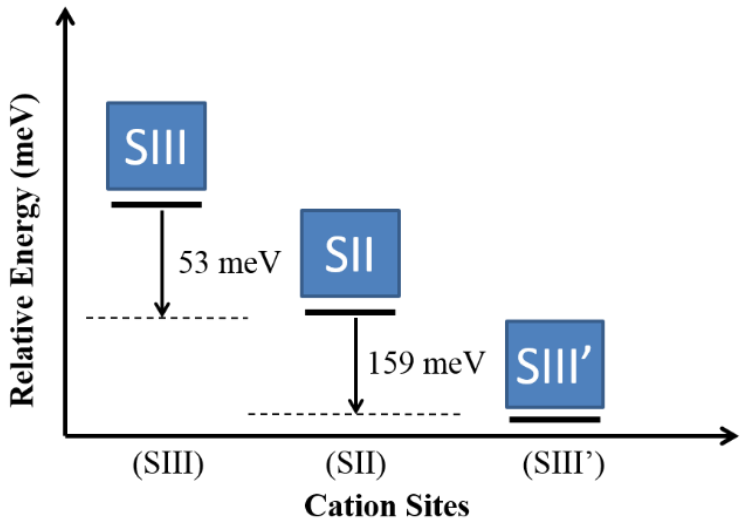

Fig. 3. Relative total energy of **r35**CsCHA crystals with Cs^+ cation located at different sites. Site SIII' is the most stable cation site for Cs^+.

In order to examine if the site preference in the **r35**CsCHA applies to that in the **r3**CsCHA, we carried out two sets of calculations. The first set includes three different configurations. The first configuration has all nine Cs^+ cations located at the nine SIII' sites. In the second and third configurations, one Cs^+ cation is moved from SIII' to SII and SIII, respectively. Table 1 compares the total energy results, showing an occupation sequence, i.e., SIII' > SII > SIII, similar to that in **r35**CsCHA, despite the increased cation density. This agreement suggests that the coexistence of multiple Cs^+ cations in one unit cell does not affect the site preference of a single Cs^+ cation.

In our second set of calculations, we moved one, two, and three Cs^+ cations from SIII' to site II, respectively. Table 2 lists the total energy results. Clearly all nine Cs^+ cations prefer to sit at site III'. This cation distribution pattern agrees well with our recent experimental results on Cs-exchanged chabazite with a Si/Al ratio of ~2.5 as determined by synchrotron powder XRD [5]. A previous experimental study showed that Cs^+ cations preferentially occupy all the SIII' sites in a dehydrated Cs form chabazite with similar Si/Al ratio of ~2.5 [24]. Another experimental study also showed that large cation, K^+ therein, favours site SIII' in a chabazite with Si/Al ratio of ~2.5 [25], which is also consistent with our results in **r3**CsCHA. The excellent agreement with experimental results justifies the reliability of our structural models and DFT computational approach, allowing us to carry out further computational studies to reveal material properties and in-depth fundamental gas admission mechanism that cannot be captured by the use of experimental methods.

Cs^+ cation stably coordinates at site SIII' and is unlikely to hop to other sites under ambient temperature. Our previous *in situ* synchrotron PXRD experimental study clearly showed that Cs^+ cation stably coordinates at the pore aperture site (site SIII') with an 100% site occupancy up to 303 K [5]. Interestingly, the immobile behaviour of Cs^+ cation is different from the mobile Na^+ cation in MOR zeolite [26]. This could be because Cs^+ cation is heavier and larger than Na^+ cation.

Table 1. DFT total energy results for the **r3**CsCHA unit cell with eight Cs^+ cations located at SIII' and the ninth Cs^+ cation located at SIII', SII, and SIII, respectively.

Cs distribution	9 Cs^+ (SIII')	8 Cs^+ (SIII') 1 Cs^+ (SII)	8 Cs^+ (SIII') 1 Cs^+ (SIII)
Total Energy (eV)	-872.696	-872.188	-871.578

Table 2. DFT total energy results for the **r3**CsCHA unit cell with Cs^+ cations distributed at SIII' and SII sites.

Cs distribution	9 Cs^+ (SIII')	8 Cs^+ (SIII') 1 Cs^+ (SII)	7 Cs^+ (SIII') 2 Cs^+ (SII)	6 Cs^+ (SIII') 3 Cs^+ (SII)
Total Energy (eV)	-872.696	-872.188	-871.792	-871.152

3.3 Determination of Cs^+ Cation Movement Path

As the relative stability of different cation sites is clear, we can propose possible path for cation movement upon gas adsorption. Note that the most stable site SIII' directly relates to gas admission through a chabazite 8MR aperture. In our previous work we proposed that for gas molecules such as CO_2, N_2, and CH_4 to pass through an 8MR pore aperture, the door-keeping cation (e.g., Cs^+ residing at SIII') has to move away from this site [5]. Given site SII represents the second most stable site for Cs^+ cation following site SIII', we treated the path from SIII' to SII as cation movement path. No matter if the cation permanently moves from SIII' to SII (migration) or temporarily and reversibly moves away from SIII' toward SII (deviation), we can use the energy barrier associated with the cation movement path to assess the difficulty for this process to occur.

We started from the relatively simple case – Cs^+ movement in **r35**CsCHA. Using NEB method, we calculated the energy barrier ΔE_b for one Cs^+ cation moving from site SIII' to site SII (shown in Fig. 4a). Clearly, the Cs^+ cation has to climb a "hill" between site SIII' and site SII in order to reach this second most stable site (Fig. 4b).

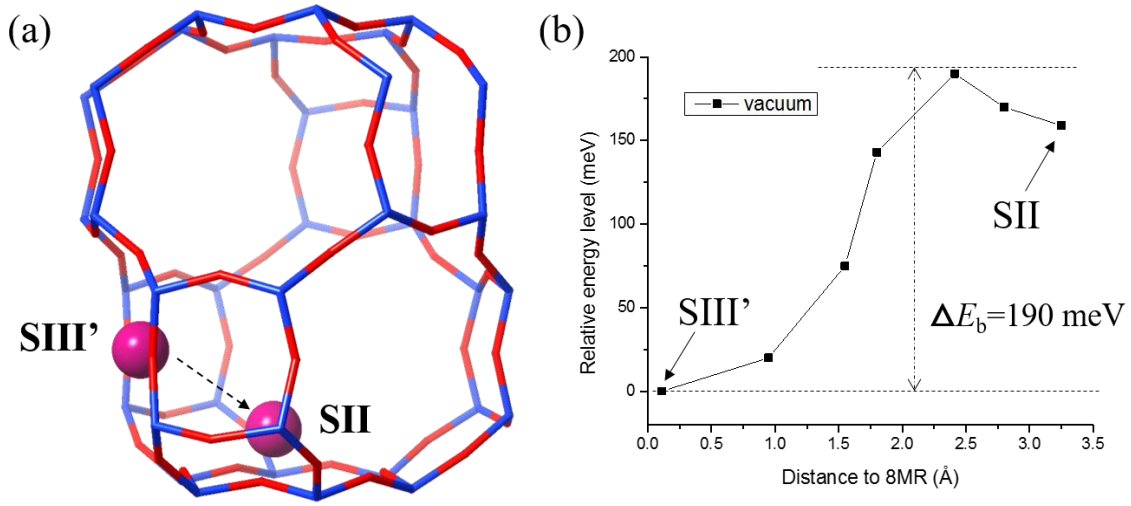

Fig. 4. (a) Sketch to illustrate the migration path of Cs^+ from SIII' to SII in case of **r35**CsCHA. (b) Relative total energy results at different positions in the migration path calculated by using the NEB method.

Determining the ΔE_b for Cs^+ migration in **r3**CsCHA would be more complicated because various Al distribution possibilities should affect the energy barrier results. Due to uneven Si/Al distribution, **r3**CsCHA has different 8MRs and 6MRs in terms of different number of Al atoms contained in a given ring, leading to different stability for Cs^+ cation at different sites SIII' and SII, respectively. For example, there exist 8MRs containing one, two, and three Al atoms, respectively; and 6MRs containing one and two Al atoms, respectively. The combination of various pairs of 8MR and 6MR, in principle, should lead to different energy barrier results. Among them, the lowest one is the most important case since the 8MRs would be opened (resulting from the cation migration) at a lower temperature to admit gas molecules. Unfortunately, it is very time consuming to do DFT NEB calculations for all cases to identify the one with the lowest energy barrier. A time efficient semi-quantitative method is desirable.

We note that in the case of **r35**CsCHA, the energy barrier (ΔE_b) of 190 meV is comparable to the energy difference (ΔE) between sites SIII' and SII, namely, 159 meV (Fig. 3). In addition, the cation migration path is in the vicinity of the 8MR and 6MR. We postulate that the energy barrier and energy difference should be largely determined by the structure of these two rings (i.e., different number of Al atoms). There should be a correlation between ΔE_b and ΔE. Therefore, here we proposed to use ΔE as a semi-quantitative measure for the energy barrier ΔE_b to characterize the difficulty in cation movement (from SIII' towards SII). Figure 5 shows the energy difference in all six types of pair combinations of 8MR and 6MR. A Cs^+ cation migration from a 3-Al-contained 8MR to a 1-Al-contained 6MR yields the highest energy difference (938 meV). The cation migration from a 2-Al-contained 8MR to a 2-Al-contained 6MR (501 meV) or from a 1-Al-contained 8MR to a 2-Al-contained 6MR (508 meV) has a quite close small ΔE value. Since cation energetically favours to coordinate to a ring with more charges via substitution of Si atom by Al atom, a cation migration from an Al-rich 8MR to an Al-lean 6MR should experience the largest ΔE and vice versa. This is in a general consistency with our DFT results.

We carried out NEB calculation for ΔE_b for Cs^+ cation migration under vacuum for 1-Al-contained 8MR to a 2-Al-contained 6MR. The resulting energy barrier (ΔE_b = 651 meV) (Fig. 7) is comparable to the corresponding energy difference (ΔE = 508 meV) (Fig. 5), indicating

that ΔE can be adopted as a convenient semi-quantitative measure to efficiently determine the migration path with the smallest ΔE_b.

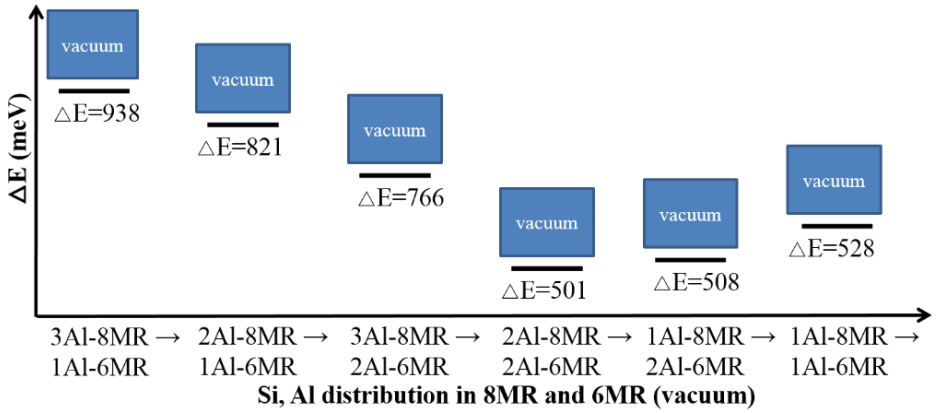

Fig. 5. The influence of uneven Si and Al distribution on the energy difference ΔE for Cs^+ occupancy at SIII' and SII in **r3**CsCHA (in vacuum).

The above discussion is for a bare **r3**CsCHA system. The presence of gas molecules could change ΔE (and the ΔE_b) results. Figure 6 shows the energy difference ΔE results of the case where one CO_2 molecule was placed near the migration path. The presence of CO_2 leads to remarkably reduced ΔE. The relative energy order remains similar to the vacuum case – cation migration from Al-richer 8MRs to Al-leaner 6MRs exhibiting a higher ΔE value. This consistency suggests that the combination of a 1-Al-contained 8MR to a 2-Al-contained 6MR is the migration path for Cs^+ with the least thermal activation. In next section, we carried out NEB calculations for this case to accurately determine the ΔE_b.

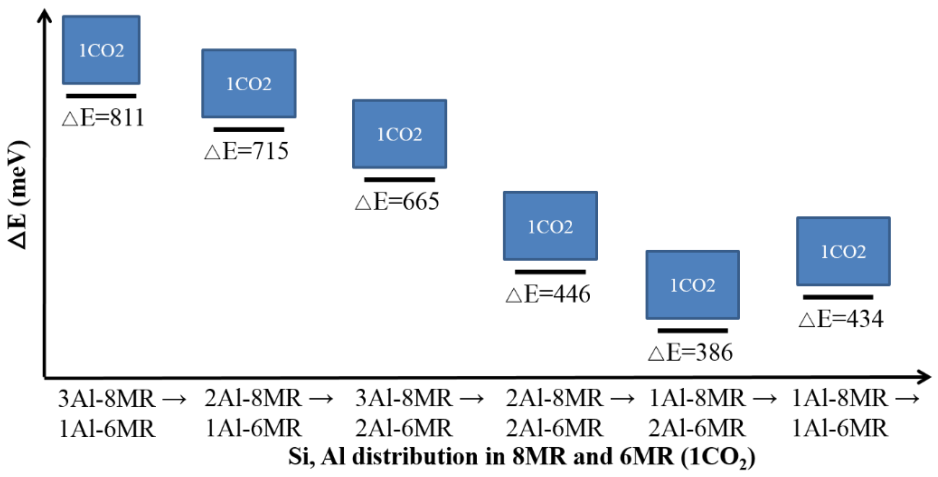

Fig. 6. The influence of uneven Si and Al distribution on the energy difference ΔE for Cs^+ occupancy at SIII' and SII in the presence of one CO_2 in one **r3**CsCHA unit cell.

3.4 The Effect of Gas Molecules on Cation Movement

In this section, we consider the influence of CO_2, N_2, and CH_4 on the magnitude of the energy barrier ΔE_b for cation movement along the easiest path. We performed NEB calculations to straightforwardly examine the effect of gas on the energy barrier associated with cation movement path identified in the last section (from the 1-Al contained 8MR (SIII') to the 2-Al contained 6MR (SII)) for selected typical cases. Specifically, we studied the effect of CO_2 in detail by considering three different gas concentrations. For N_2 and CH_4, we only considered two concentrations and one concentration, respectively. The results are shown in Fig. 7. Notably, CO_2 significantly reduces the energy barrier for cation migration with respect to vacuum and a higher CO_2 concentration leads to larger extent of reduction in the energy barrier. In contrast, both N_2 and CH_4 impart negligible effect in reducing the energy barrier for cation migration.

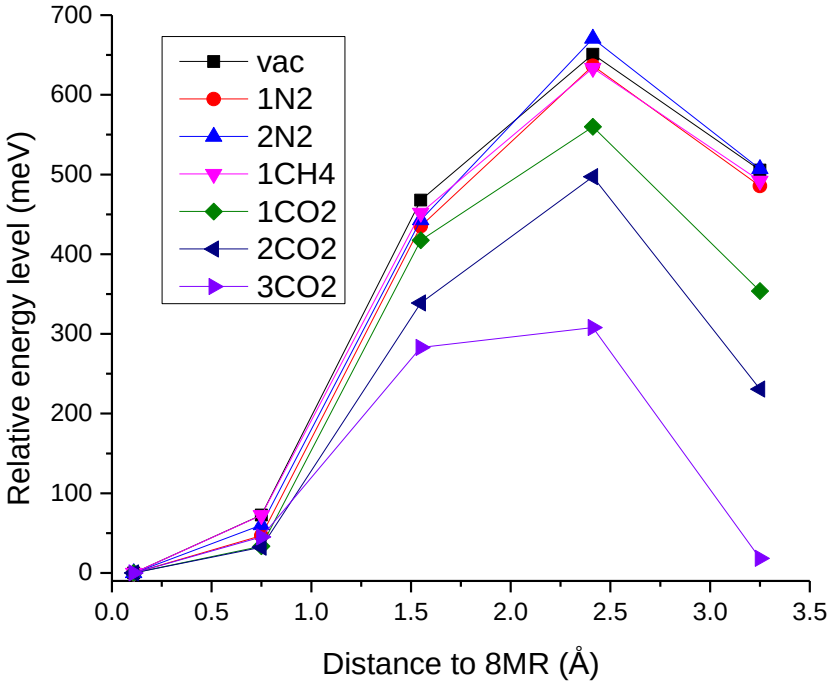

Fig. 7. The effect of different gases on the energy barrier ΔE_b for one Cs^+ cation movement from SIII' to SII in **r3**CsCHA.

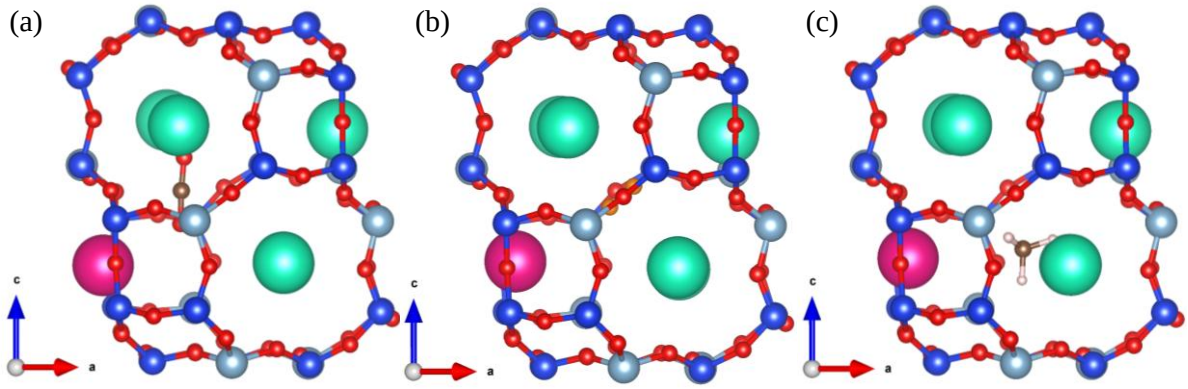

Fig. 8. The gas-adsorbent adsorption complexes in the cases of (a) CO_2-**r3**CsCHA, (b) N_2-**r3**CsCHA, and (c) CH_4-**r3**CsCHA. Color scheme: Red, O; Blue: Si; Grey, Al; Aqua and violet, Cs; brown: C; Light grey: N: orange; H: light pink.

To further justify the viability of using energy difference to represent energy barrier, we also calculated the energy difference results for above cases. For each case, we calculated the total energy of the fully relaxed configuration of gas-chabazite complex with the Cs^+ cation at the center of 1-Al contained 8MR (SIII') or above the 2-Al contained 6MR (SII), labelled E_{total}(SIII') and E_{total}(SII), respectively. The gas concentrations correspond to one, two, or three gas molecules per unit cell. We then simply recorded the absolute difference between the total energy with Cs^+ at SIII' and that with Cs^+ at SII as the energy difference, i.e., $\Delta E_b = |E_{total}(SIII') - E_{total}(SII)|$. As shown in Table 3, CO_2 significantly lowers the energy difference with respect to vacuum and increasing the gas concentration strengthens this effect: at 1 CO_2 per unit cell reduces approximately 25%; 2 CO_2 approximately 50%; 3 CO_2 more than 90%. In contrast, neither N_2 nor CH_4 could effectively lower the energy difference compared with vacuum, even if the gas concentration is elevated. Clearly, the energy difference gives the same trend in the effect of gas molecules on the difficulty for cation migration determined by the energy barrier, consolidating this semi-quantitative method of using ΔE to represent ΔE_b.

To illustrate the interaction between different gases and chabazite, Figure 8 shows geometry of adsorbate-adsorbent interaction complex of their most stable configurations with Cs^+ cation at the 8MR site (SIII'). The binding energy values (calculated at the optB86b-vdW level) are 51.62, 31.94, 44.42 kJ/mol for CO_2, N_2, and CH_4 respectively. The adsorbate-Cs distance values are 3.15 Å (between Cs^+ and the nearest O of CO_2), 3.82 Å (between Cs^+ and

the nearest N of N_2), and 3.69 Å (between Cs^+ and the nearest H of CH_4). It should be noted that the sequence of binding energy of different gases are not directly correlated to the sequence of reduced energy barrier for cation migration. This is because the binding energy reflects the total interaction between the adsorbate and the whole adsorbent (including both the framework and extraframework cation). We contend that there might be a correlation between the Cs-adsorbate interaction and the energy barrier associated to cation migration. However, DFT calculates cannot extract the Cs-adsorbate interaction from the total binding energy. We will attempt to solve this problem in the future work.

Table 3. The effect of different gases on the energy difference (in meV) between SIII' and SII in **r3**CsCHA.

Atmosphere / **NO. of molecules**	**CO_2**	**N_2**	**CH_4**
0	508	508	508
1	386	500	501
2	262	501	551
3	45	450	445

Overall, our calculations suggest that CO_2 has the strongest ability to reduce the energy barrier for cation movement with respect to under vacuum, while N_2 and CH_4 have nearly no ability to lower this energy barrier. Increasing the gas concentration magnifies the effect of CO_2 but has no influence on N_2 or CH_4. We attribute the effect of gases on inducing the cation movement to their polarity. CO_2 has strong quadrupole and high polarisability, which enables it to strongly interact with the Cs^+ cation and to flatten the potential energy well of the cation. On the other hand, N_2 has smaller quadrupole and polarisability than CO_2, and CH_4 only has smaller polarisability than CO_2, making these two gases interact with the cation too weakly to change its potential energy well.

3.5 The Effect of Dispersion Correction on the Cation Movement

Dispersion force plays an indispensable part in the interaction between gas molecules and zeolites [27], as it contributes to the binding energy to some extent. However, it is yet to be known if the contribution from dispersion affects the relative energies between different configurations. We adopted a vdW-DF scheme – optB86b-vdW – to examine its effect on the

energy difference by selecting the typical cases in **r3**CsCHA: vacuum, 1 CH_4 per unit cell, 1 N_2 per unit cell, 1 CO_2 per unit cell, 2 CO_2 per unit cell, and 3 CO_2 per unit cell. The optB86b-vdW scheme represents a typical vdW method as we have determined that it is the most appropriate one in accounting for our gas-chabazite system in a previous study [21]. The results (shown in Fig. 9) clearly show that incorporation of dispersion doses not change the trend of energy difference under any atmosphere; it only lowers the magnitude of the respective energy difference to a similar extent, i.e., ~ 50 meV. This indicates that the dispersion background created by the zeolite framework keeps generally unvaried for the cation and gas molecules at least for the starting (Cs^+ at SIII') and ending (Cs^+ at SII) configurations of the cation migration path. Therefore, we can safely use results calculated at pure DFT level (PBE level) for evaluation of energy barriers in our system, which effectively cuts the computational cost.

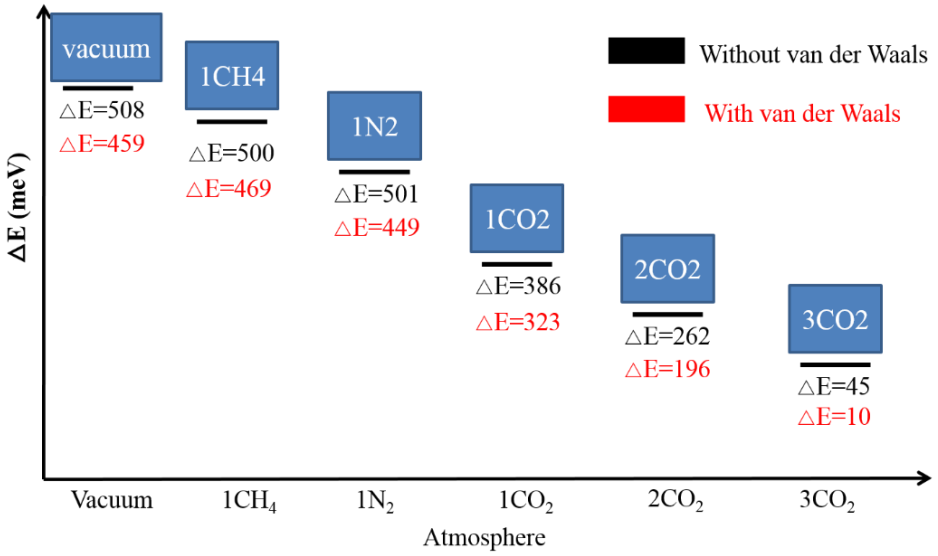

Fig. 9. The effect of vdW dispersion on the energy difference in **r3**CsCHA.

3.6 Assessment of viability of trapdoor mechanism to other gas molecules

In the end of this paper, we would like to utilise the ΔE (semi-quantitative measure of ΔE_b) to examine the viability of trapdoor mechanism on some other gas molecules, such as H_2, CO, H_2O, H_2S, N_2O, C_2H_2, and O_2.

Table 4 summarises the results. H_2 has a weak interaction with Cs^+ cation owning to its relatively low polarisability. In contrast, CO is a strong molecule due to its relatively high polarisability and dipole. Thus, H_2 imparts negligible effect on the energy difference for Cs^+ movement, reflected by the energy difference value of 498 meV for 1 H_2 molecule per unit cell comparable to under vacuum (508 meV), 1 N_2 (501 meV), and 1 CH_4 (500 meV). On the other hand, CO substantially reduces the energy difference for Cs^+ movement, reflected by 283 meV for 3 CO molecules per unit cell, which, although not as effective as 3 CO_2 (45 meV), already sufficiently effective in inducing cation movement with respect to under vacuum as well as N_2 and CH_4. In a similar way, gas molecules with relatively high polarity such as H_2O, H_2S, N_2O, and C_2H_2 lowers the energy difference to different extents, while O_2 with relatively low polarity hardly affects the energy difference. These results suggest that trapdoor **r3**CsCHA could be employed to separate the CO, H_2O, H_2S, N_2O, and C_2H_2 from the H_2, O_2, N_2, and CH_4. Further experimental studies are required to justify our conclusions.

Table 4. The effect of other gases on the energy difference associated to cation movement from site SIII' to SII.

Atmosphere	1 CO	3 CO	1 H_2	1 H_2O	1 H_2S	1 N_2O	1 C_2H_2	1 O_2
ΔE (meV)	477	283	498	242	351	356	446	455

4. Conclusions

We have employed density functional theory calculations to demonstrate that the "door-keeping" Cs^+ cation has to pay an energy penalty to move away from the center of 8MR pore aperture (thus allow gas admission) in a typical trapdoor zeolite – **r3**CsCHA. The difficulty of this "door-open" process can be reflected by the energy barrier associated with the cation movement path from its most stable position (site SIII') to the second most stable one (site SII) inside the chabazite supercavity. The energy difference between these two configurations can qualitatively feature the actual energy barrier. The presence of "strong" gas molecules that possess "strong" interaction strength owning to relatively high polarity, such as CO_2 and CO, can substantially lower the energy difference, whereas those "weak" molecules, such as N_2, CH_4, and H_2, can hardly change the energy difference. The incorporation of van der Waals dispersion does not compromise the above argument. Therefore, we conclude that

different gases has different abilities to affect the movement of the door-keeping cation in Cs-exchanged chabazite, reflected by the energy difference between the total energies of the starting and ending configurations. This study lays a concrete theoretical foundation for our proposed "molecular trapdoor" mechanism [5] and directs the theoretical route for further investigation of other novel trapdoor materials.

Acknowledgement

This research was undertaken with the assistance of resources from the National Computational Infrastructure (NCI), which is supported by the Australian Government. J.S., P.A.W., and J.Z.L acknowledge the Australian Research Council for providing the funding (DP2013000024). G.L. is the recipient of an Australian Research Council Discovery Early Career Researcher Award (DE140101824).

Author contributions

J.S., P.A.W. and J.Z.L. conceived and designed the molecular simulation study. J.S. and J.Z.L. conducted the *ab initio* DFT calculations and J.S., G.L., P.A.W., and J.Z.L., analyzed the data. J.S. and G.L. wrote the paper. All authors discussed the results and commented on the manuscript.

Conflict of Interest: The authors declare that they have no conflict of interest.

References

[1] K. Lee, É.D. Murray, L. Kong, B.I. Lundqvist, D.C. Langreth, Higher-accuracy van der Waals density functional, Physical Review B, 82 (2010) 081101.
[2] J. Shang, G. Li, J. Li, L. Li, P.A. Webley, J.Z. Liu, Density Functional Theory Computational Study of Alkali Cation-Exchanged Sodalite-like Zeolitelike Metal–Organic Framework for CO2, N2, and CH4 Adsorption, The Journal of Physical Chemistry C, 119 (2015) 27449-27456.
[3] T. Ohgushi, K. Ishimaru, Y. Adachi, Movements and Hydration of Potassium Ion in K-A Zeolite, The Journal of Physical Chemistry C, 113 (2009) 2468-2474.
[4] D.W. Breck, Zeolite Molecular Sieves: Structure, Chemistry, and Use, Wiley, New York, 1974.
[5] J. Shang, G. Li, R. Singh, Q. Gu, K.M. Nairn, T.J. Bastow, N. Medhekar, C.M. Doherty, A.J. Hill, J.Z. Liu, P.A. Webley, Discriminative Separation of Gases by a "Molecular Trapdoor" Mechanism in Chabazite Zeolites, J. Am. Chem. Soc., 134 (2012) 19246-19253.

[6] J. Shang, G. Li, R. Singh, P. Xiao, J.Z. Liu, P.A. Webley, Determination of Composition Range for "Molecular Trapdoor" Effect in Chabazite Zeolite, The Journal of Physical Chemistry C, 117 (2013) 12841-12847.
[7] J. Shang, G. Li, Q. Gu, R. Singh, P. Xiao, J.Z. Liu, P.A. Webley, Temperature controlled invertible selectivity for adsorption of N2 and CH4 by molecular trapdoor chabazites, Chem. Commun., 50 (2014) 4544-4546.
[8] O.V. Yakubovich, W. Massa, P.G. Gavrilenko, I.V. Pekov, Crystal structure of chabazite K, Crystallogr. Rep., 50 (2005) 544-553.
[9] J. Shang, G. Li, R. Singh, P. Xiao, J.Z. Liu, P.A. Webley, Potassium Chabazite: A Potential Nanocontainer for Gas Encapsulation, J. Phys. Chem. C., 114 (2010) 22025-22031.
[10] W.J. Mortier, J.J. Pluth, J.V. Smith, Positions of cations and molecules in zeolites with the chabazite framework I. Dehydrated ca-exchanged chabazite, Mater. Res. Bull., 12 (1977) 97-102.
[11] W.J. Mortier, J.J. Pluth, J.V. Smith, Positions of cations and molecules in zeolites with the chabazite framework III. Dehydrated Na-exchanged chabazite, Mater. Res. Bull., 12 (1977) 241-249.
[12] M. Calligaris, A. Mezzetti, G. Nardin, L. Randaccio, Cation sites and framework deformations in dehydrated chabazites. Crystal structure of a fully silver-exchanged chabazite, Zeolites, 4 (1984) 323-328.
[13] P. Xiao, J. Zhang, P. Webley, G. Li, R. Singh, R. Todd, Capture of CO2 from flue gas streams with zeolite 13X by vacuum-pressure swing adsorption, Adsorption, 14 (2008) 575-582.
[14] F. Göltl, J. Hafner, Alkane adsorption in Na-exchanged chabazite: The influence of dispersion forces, J. Chem. Phys., 134 (2011) 0641021-06410211.
[15] G. Kresse, J. Furthmüller, Efficient iterative schemes for ab initio total-energy calculations using a plane-wave basis set, Phys. Rev. B, 54 (1996) 11169-11186.
[16] J.P. Perdew, K. Burke, M. Ernzerhof, Generalized Gradient Approximation Made Simple, Phys. Rev. Lett., 77 (1996) 3865-3868.
[17] G. Kresse, D. Joubert, From ultrasoft pseudopotentials to the projector augmented-wave method, Phys. Rev. B, 59 (1999) 1758-1775.
[18] F. Celestini, G. Kirstetter, Effect of an electric field on a Leidenfrost droplet, Soft Matter, 8 (2012) 5992-5995.
[19] P.S. Bárcia, L. Bastin, E.J. Hurtado, J.A.C. Silva, A.E. Rodrigues, B. Chen, Single and Multicomponent Sorption of CO_2, CH_4 and N_2 in a Microporous Metal-Organic Framework, Sep. Purif. Technol., 43 (2008) 3494-3521.
[20] G.G. Wells, R. Ledesma-Aguilar, G. McHale, K. Sefiane, A sublimation heat engine, Nat Commun, 6 (2015).
[21] J. Shang, G. Li, R. Singh, P. Xiao, D. Danaci, J.Z. Liu, P.A. Webley, Adsorption of CO2, N2, and CH4 in Cs-exchanged chabazite: A combination of van der Waals density functional theory calculations and experiment study, The Journal of Chemical Physics, 140 (2014) 084705.
[22] K. Sumida, D.L. Rogow, J.A. Mason, T.M. McDonald, E.D. Bloch, Z.R. Herm, T.-H. Bae, J.R. Long, Carbon Dioxide Capture in Metal–Organic Frameworks, Chem. Rev., 112 (2012) 724-781.
[23] B. Civalleri, A.M. Ferrari, M. Llunell, R. Orlando, M. Mérawa, P. Ugliengo, Cation Selectivity in Alkali-Exchanged Chabazite: An ab Initio Periodic Study, Chem. Mat., 15 (2003) 3996-4004.
[24] M. Calligaris, A. Mezzetti, G. Nardin, L. Randaccio, Crystal structures of the hydrated and dehydrated forms of a partially cesium-exchanged chabazite, Zeolites, 6 (1986) 137-141.

[25] L.J. Smith, H. Eckert, A.K. Cheetham, Potassium Cation Effects on Site Preferences in the Mixed Cation Zeolite Li,Na-Chabazite, Chem. Mat., 13 (2001) 385-391.
[26] T. Bučko, J. Hafner, The role of spatial constraints and entropy in the adsorption and transformation of hydrocarbons catalyzed by zeolites, J. Catal., 329 (2015) 32-48.
[27] R.E. Morris, J. Cejka, Exploiting chemically selective weakness in solids as a route to new porous materials, Nat Chem, 7 (2015) 381-388.